



# Research on accurate virtual trajectory length model for TGS transmission measurement

Rong-Rong Su<sup>1</sup> · San-Gang Li<sup>1,2</sup> · Chu-Xiang Zhao<sup>1</sup> · Li Yang<sup>3</sup> · Ming-Zhe Liu<sup>1,2</sup> · Shan Liao<sup>1</sup> · Zhi Zhou<sup>1</sup> · Qing-Shan Tan<sup>1</sup> · Zhi-Xing Gu<sup>1</sup> · Xian-Guo Tuo<sup>4</sup> · Yi Cheng<sup>1</sup>

Received: 27 December 2023 / Revised: 25 April 2024 / Accepted: 29 April 2024 / Published online: 28 January 2025

© The Author(s), under exclusive licence to China Science Publishing & Media Ltd. (Science Press), Shanghai Institute of Applied Physics, the Chinese Academy of Sciences, Chinese Nuclear Society 2024

## Abstract

To accurately reconstruct the tomographic gamma scanning (TGS) transmission measurement image, this study optimized the transmission reconstruction equation based on the actual situation of TGS transmission measurement. Using the transmission reconstruction equation and the Monte Carlo program Geant4, an innovative virtual trajectory length model was constructed. This model integrated the solving process for the trajectory length and detection efficiency within the same model. To mitigate the influence of the angular distribution of  $\gamma$ -rays emitted by the transmitted source at the detector, the transport processes of numerous particles traversing a virtual nuclear waste barrel with a density of zero were simulated. Consequently, a certain amount of information was captured at each step of particle transport. Simultaneously, the model addressed the nonuniform detection efficiency of the detector end face by considering whether the energy deposition of particles in the detector equaled their initial energy. Two models were established to validate the accuracy and reliability of the virtual trajectory length model. Model 1 was a simplified nuclear waste barrel, whereas Model 2 closely resembled the actual structure of a nuclear waste barrel. The results indicated that the proposed virtual trajectory length model significantly enhanced the precision of the trajectory length determination, substantially increasing the quality of the reconstructed images. For example, the reconstructed images of Model 2 using the “point-to-point” and average trajectory models revealed a signal-to-noise ratio increase of 375.0% and 112.7%, respectively. Thus, the virtual trajectory length model proposed in this study holds paramount significance for the precise reconstruction of transmission images. Moreover, it can provide support for the accurate detection of radioactive activity in nuclear waste barrels.

**Keywords** Tomographic gamma scanning · Transmission measurement reconstruction · Geant4 · Trajectory length model · Nonuniform detection efficiency

This work was supported by The Youth Science Foundation of Sichuan Province (Nos. 2022NSFSC1230, 2022NSFSC1231, and 23NSFSC5321) and the Science and Technology Innovation Seedling Project of Sichuan Province (No. MZGC20230080) and the General project of national Natural Science Foundation of China (No. 12075039) and the Youth Science Foundation of China (No. 12105030) and the Key project of the National Natural Science Foundation of China (No. U19A2086).

✉ San-Gang Li  
lisangang@cdut.edu.cn

<sup>1</sup> College of Nuclear Technology and Automation Engineering, Chengdu University of Technology, 1#, Dongsanlu, Erxianqiao, Chengdu 610059, China

<sup>2</sup> Applied Nuclear Technology in Geosciences Key Laboratory of Sichuan Province, (Chengdu University of Technology), 1#, Dongsanlu, Erxianqiao, Chengdu 610059, China

## 1 Introduction

Tomographic gamma scanning (TGS) has undergone substantial improvements and development based on segmented gamma scanning (SGS) technology. The SGS, which divides the measured waste barrel into multiple segments, assuming

<sup>3</sup> University of Science and Technology of China, Hefei 230026, China

<sup>4</sup> School of Physics and Electronic Engineering, Sichuan University of Science and Engineering, Zigong 643000, China

a uniform distribution of the medium in each segment, cannot satisfy the demands of actual nuclear waste barrels. Its effectiveness has been demonstrated only for the detection of low-density or known medium- to high-density uniformly distributed nuclear waste barrels [1–3]. Consequently, TGS has evolved from two-dimensional scanning to three-dimensional scanning based on SGS. When conducting axial segmented scanning on nuclear waste barrels, TGS introduces translational and rotational scanning on each segment, thereby providing information on the “depth” of nuclear waste barrels that SGS technology cannot [4, 5]. TGS can detect the distribution of media in nuclear waste barrels and extend the detection range of nondestructive analysis technology to nonuniformly distributed medium- and high-density nuclear waste barrels [6].

The TGS technology involves transmission and emission measurements [7, 8]. During the transmission measurements, the nuclear waste barrel is divided into several voxels. The transmission data measured by the detector are then used to reconstruct the line attenuation coefficient of each voxel using a reconstruction algorithm [9]. The emission measurement process is aimed at obtaining a radioactive intensity distribution map within a nuclear waste barrel [10]. To ensure the accuracy of the obtained radioactive intensity distribution, an attenuation coefficient derived from the transmission measurement process must be applied [11]. This coefficient facilitates meticulous point-by-point corrections for self-absorption. Thus, the accuracy of the line attenuation coefficient reconstructed from the transmission measurements is pivotal and directly influences the accuracy of the radioactive intensity distribution map obtained from the emission measurements [12–14].

To reconstruct the line attenuation coefficient, Estep et al. from Los Alamos National Laboratory in the USA simplified the physical model of the TGS transmission measurement [15]. The transmission source and detector were treated as dimensionless point sources and detectors, respectively. The ray beam emitted by the point source was regarded as a parallel beam. The simplified model was referred to as a “point-to-point” model [16]. This model has significantly simplified the calculation of the line attenuation coefficient, and currently serves as the mainstream model for calculating the trajectory length. However, in an actual TGS system,  $\gamma$ -rays at a certain cone angle are emitted by the transmission source and pass through the nuclear waste barrel. This results in a corresponding angle for the large detector. With the translation and rotation of the transmission source and detector (or nuclear waste barrel) during the transmission measurement process, the distribution of the trajectory length of the rays passing through the voxels changes accordingly [17]. The disparity between the “point-to-point” model and the actual device yields a significant error between the computed trajectory length and the trajectory length of the actual rays

passing through the voxel. Consequently, the image quality in transmission measurement reconstruction is significantly degraded.

Further, considering the angular distribution of emitted  $\gamma$ -rays on the detector in TGS systems, certain studies have proposed various models to solve the trajectory length. Lei from the Chengdu University of Technology developed a Monte Carlo simulation calculation model based on surface flux. Quanhu from the Institute of Atomic Energy proposed an average trajectory model. Further, Miaomiao from the Harbin Engineering University proposed a “point-detector (PD)” model for solving the average trajectory. However, these models do not consider the practical scenario of a detector detecting emitted rays, and the detection efficiency of  $\gamma$ -rays varies at different positions on the detector end face (an uneven response) [18].

To reduce the impact of uneven responses, Quanhu from the Atomic Energy Institute proposed a Monte Carlo trajectory length model based on the Cyrus–Beck algorithm. The test results demonstrated confirmed the superiority of this model over the average trajectory and the “point-to-point” models [19]. Nevertheless, the trajectory length solved by this model is related to the barreled medium and cannot be determined in advance. Repeated MC simulations are required to obtain the trajectory length, thereby rendering the calculation process complex. Moreover, for samples with medium- to high-density media, significant errors are obtained [20]. In addition, as the model does not consider the structural parameters of the actual nuclear waste barrel and the beam limiting effect of the collimator used in High Purity Germanium (HPGe) detectors, it is not suitable for practical applications and further research is needed [21]. Although this model has various shortcomings, its research results indicate that reducing the impact of the uneven detection response of the detector end face is an effective method for improving the accuracy of the trajectory length.

This study optimized the transmission reconstruction equation according to an actual TGS transmission measurement situation, which considered the angular distribution of  $\gamma$ -rays emitted from the transmission source on the detector and varying the detection efficiency when they reached different points on the detector end face. To obtain the equivalent trajectory length matrix elements and the detection efficiency of the optimized transmission image reconstruction equation, a virtual trajectory length model was proposed based on Geant4. Leveraging the capability of the Monte Carlo program Geant4, which can simulate the transport process of numerous particles and capture information at each step, the transport of particles emitted by a transmission source passing through a virtual waste barrel with a density of 0 were simulated. Considering the varying detection efficiencies at different points on the detector end face, we determined whether the detection of particles by the detector was based on the energy deposition

of each particle in the detector being equal to its initial energy. This virtual model reduced the impact of the uneven response function on the detector’s end-face detection efficiency, providing a simple and accurate solution for the trajectory length.

## 2 Method

### 2.1 Optimization of transmission reconstruction equation

In traditional TGS transmission measurements, the transmission reconstruction equation is expressed as Eq. (1) [22]:

$$\sum_{j=1}^n \mu_j T_{ij} = p_i \tag{1}$$

where  $p_i$  is the negative logarithm of the  $\gamma$ -rays transmittance at the  $i$ -th transmission measurement position, also known as projection. Further,  $T_{ij}$  is the trajectory length of the  $j$ -th voxel that the  $\gamma$ -rays pass through at the  $i$ -th position,  $\mu_j$  is the line attenuation coefficient of the  $j$ -th voxel, and  $n$  is the total number of voxels.

In actual TGS transmission measurements,  $\gamma$ rays emitted by the transmission source exhibit an angular distribution, and the detection efficiencies of all points on the detector end face are not the same. The TGS transmission formula is expressed as follows [23].

$$p_i = \frac{1}{\sum_{k=1}^N \epsilon_k} \sum_{k=1}^N \left[ \epsilon_k \exp \left( \sum_{j=1}^n (-x_{ikj} \mu_j) \right) \right] \tag{2}$$

where  $p_i$  is the transmissivity at the  $i$ -th position,  $\epsilon_k$  is the detection efficiency of the  $k$ -th point on the detector end face for a certain energy  $\gamma$ -rays,  $x_{ikj}$  is the length of the trajectory where the ray, passing through the  $k$ -th point of the detector end face, intersects the  $j$ -th voxel at the  $i$ -th measurement position, and  $N$  is the total number of  $\gamma$ -rays emitted by the transmission source within the solid angle of the detector.

Further,

$$q_k = \exp \left( \sum_{j=1}^n (-x_{ikj} \mu_j) \right) \tag{3}$$

where  $q_k$  is the attenuation rate at which the  $k$ th ray passes through the material without considering the detector efficiency.

Thus, Eq. (4) can be obtained as

$$p_i \sum_{k=1}^N \epsilon_k = \sum_{k=1}^N \epsilon_k q_k \tag{4}$$

Next, we obtain Eq. (5) by considering the negative logarithms of both sides of Eq. (3):

$$-\ln q_k = \sum_{j=1}^n x_{ikj} \mu_j \tag{5}$$

Then:

$$\begin{bmatrix} x_{i11} & x_{i12} & x_{i13} & \dots & x_{i1n} \\ x_{i21} & x_{i22} & x_{i23} & \dots & x_{i2n} \\ \vdots & \vdots & \vdots & \dots & \vdots \\ \vdots & \vdots & \vdots & \dots & \vdots \\ x_{iN1} & x_{iN2} & x_{iN3} & \dots & x_{iNn} \end{bmatrix} \begin{bmatrix} \mu_1 \\ \mu_2 \\ \vdots \\ \vdots \\ \mu_n \end{bmatrix} = - \begin{bmatrix} \ln q_1 \\ \ln q_2 \\ \vdots \\ \vdots \\ \ln q_N \end{bmatrix} \tag{6}$$

According to Taylor’s formula, Eq. (7) can be obtained as

$$\ln q_k = (q_k - 1) - \frac{1}{2}(q_k - 1)^2 + \dots \tag{7}$$

Then:

$$\begin{bmatrix} x_{i11} & x_{i12} & x_{i13} & \dots & x_{i1n} \\ x_{i21} & x_{i22} & x_{i23} & \dots & x_{i2n} \\ \vdots & \vdots & \vdots & \dots & \vdots \\ \vdots & \vdots & \vdots & \dots & \vdots \\ x_{iN1} & x_{iN2} & x_{iN3} & \dots & x_{iNn} \end{bmatrix} \begin{bmatrix} \mu_1 \\ \mu_2 \\ \vdots \\ \vdots \\ \mu_n \end{bmatrix} = - \begin{bmatrix} \ln q_1 \\ \ln q_2 \\ \vdots \\ \vdots \\ \ln q_N \end{bmatrix} \approx -k \begin{bmatrix} q_1 - 1 \\ q_2 - 1 \\ \vdots \\ \vdots \\ q_N - 1 \end{bmatrix} \tag{8}$$

where  $k = \frac{\ln(p_i/\eta_i)}{p_i/\eta_i - 1}$  is the error correction value and  $\eta_i$  represents the detection efficiency of the detector for a certain energy  $\gamma$ -rays at the  $i$ -th measurement position.

However, Eq. (8) does not consider endpoint detection efficiency  $\epsilon_k$ . If both sides are left multiplied by the detection efficiency [28], then we obtain

$$\begin{bmatrix} \epsilon_1 & \epsilon_2 & \dots & \epsilon_N \end{bmatrix} \begin{bmatrix} x_{i11} & x_{i12} & x_{i13} & \dots & x_{i1n} \\ x_{i21} & x_{i22} & x_{i23} & \dots & x_{i2n} \\ \vdots & \vdots & \vdots & \dots & \vdots \\ \vdots & \vdots & \vdots & \dots & \vdots \\ x_{iN1} & x_{iN2} & x_{iN3} & \dots & x_{iNn} \end{bmatrix} \begin{bmatrix} \mu_1 \\ \mu_2 \\ \vdots \\ \vdots \\ \mu_n \end{bmatrix} = -k \begin{bmatrix} \epsilon_1 & \epsilon_2 & \dots & \epsilon_N \end{bmatrix} \begin{bmatrix} q_1 - 1 \\ q_2 - 1 \\ \vdots \\ \vdots \\ q_N - 1 \end{bmatrix} \tag{9}$$

Equation (9) is transformed as follows:

$$\begin{aligned} &\mu_1 \sum_{k=1}^N \epsilon_k x_{ik1} + \mu_2 \sum_{k=1}^N \epsilon_k x_{ik2} + \dots + \mu_n \sum_{k=1}^N \epsilon_k x_{ikn} \\ &= -k[(\epsilon_1 q_1 - \epsilon_1) + (\epsilon_2 q_2 - \epsilon_2) + \dots \\ &\quad + (\epsilon_N q_N - \epsilon_N)] \end{aligned} \tag{10}$$

By substituting Eq. (4) into Eq. (10), we obtain

$$\begin{aligned} &\mu_1 \sum_{k=1}^N \epsilon_k x_{ik1} + \mu_2 \sum_{k=1}^N \epsilon_k x_{ik2} + \dots + \mu_n \sum_{k=1}^N \epsilon_k x_{ikn} \\ &= k(1 - p_i) \sum_{k=1}^N \epsilon_k \end{aligned} \tag{11}$$

The equivalent trajectory length can be expressed as

$$T_{ij} = \frac{\sum_{k=1}^N \epsilon_k x_{ikj}}{\sum_{k=1}^N \epsilon_k} \tag{12}$$

The system of equations can be expressed as Eq. (13):

$$\sum_{j=1}^n \mu_j T_{ij} = \frac{\ln(p_i/\eta_i)}{p_i/\eta_i - 1} (1 - p_i) \tag{13}$$

The equation for the equivalent trajectory length, which considers the endpoint detection efficiency, is expressed as Eq. (12). By substituting the obtained equivalent trajectory lengths  $T_{ij}$ , detection efficiency  $\eta_i$ , and transmissivity  $p_i$  into Eq. (13), an equation system for the transmission image reconstruction can be obtained.

## 2.2 Model of virtual trajectory length based on Geant4

To solve the optimized transmission image reconstruction equation, the equivalent trajectory lengths, detection efficiency, and transmissivity must be obtained in advance. Transmissivity can be obtained through detector counting conversion. For detection efficiency, a passive efficiency calibration method based on the Monte Carlo method is utilized. This method requires the calculation of the detection efficiency of the detector relative to the radiation source for a certain energy gamma ray at each measurement position in advance based on the Monte Carlo method. However, studies on the solution of the equivalent trajectory length formula in Eq. (12) are scarce. The trajectory lengths obtained using Eq. (12) can be interpreted as the average length of all  $\gamma$ -rays detected by the detector passing through the  $j$ th voxel. If the trajectory lengths of all  $\gamma$ -rays passing through the  $j$ -th voxel can be calculated, then the fact whether each ray has been detected by the detector can be determined [24]. The equivalent trajectory length is obtained by averaging the trajectory lengths of the detected rays. The Monte Carlo program

Geant4 can track the trajectory lengths of each interaction step between the primary or secondary particles and matter and obtain the geometric information of each step, which provides the possibility for simulations to obtain equivalent trajectory lengths [25, 26].

To determine the equivalent trajectory length and detection efficiency, this study proposed a novel approach by constructing a virtual waste barrel and integrating the solution processes into a unified model. This model, based on Geant4, simplified the solving process and introduced a pioneering method for determining equivalent trajectory lengths. The virtual trajectory length model was structured as follows:

Based on the TGS experimental setup, a TGS simulation model without a nuclear waste barrel was constructed. The space containing the virtual waste barrel was divided into multiple segments, and one segment was selected for the simulation to calculate the equivalent trajectory length [27]. The virtual waste barrel segment was further divided into  $N \times N$  voxels, and the medium within the segment was filled with vacuum. The voxel segmentation of a single-layer nuclear waste barrel and emission status of the rays are shown in Fig. 1.

The next step involved simulating the transportation of numerous particles passing through a virtual waste barrel segment at a specific location. Leveraging Geant4 functions such as “G4Step,” “GetName(),” “GetTouchableHandle(),” and “GetPostStepPoint(),” the name of voxels traversed by the particles and the length of trajectory within these voxels were obtained. Notably, because of the absence of any

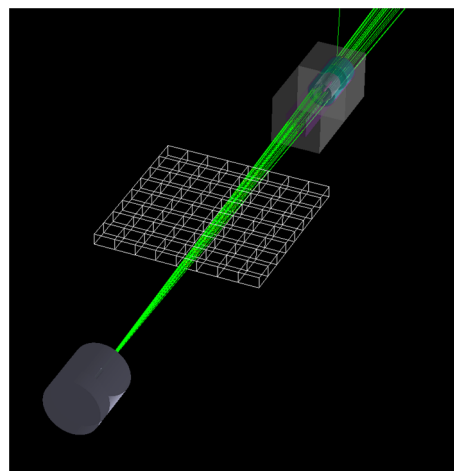


**Fig. 1** (Color online) Schematic of the virtual trajectory length model based on Geant4. The model divided the segment into  $14 \times 14$  voxels, with  $\gamma$ -rays energy set to  $E_k = 1.17$  MeV. This figure shows the situation wherein particles emitted from the radiation source passed through certain voxels. Based on Eq. (12), the model can obtain the number of particles detected by the detector on a certain voxels, as well as the cumulative sum of the trajectory lengths left by these particles on that voxel ( $\sum_{k=1}^N \epsilon_k x_{ikj}$ )

substances in the virtual waste barrel, the particle rays followed a straight-line transport path without undergoing any physical processes [29].

Considering the uneven response of the end-face detection efficiency of the detector, the simulation included a process wherein particles passing through the virtual waste barrel were detected by an HPGe detector. If the energy deposited in the detector differed from the particle’s initial energy, it was assumed that the particles were not detected, and the trajectory lengths passing through all voxels were considered as 0.

The cumulative trajectory lengths of all the particles with the same emission energy passing through the same voxel were then calculated. Dividing the total trajectory length by the number of particles with a nonzero trajectory length yielded an equivalent trajectory length corresponding to the voxel. Further, dividing the number of particles with a nonzero trajectory length at a specific energy by the total number of emitted particles at that energy yielded the detection efficiency of  $\gamma$ -rays at a particular location, denoted as  $\eta_i$ .

### 2.3 Image reconstruction algorithm

The current image reconstruction algorithms can be roughly divided into two categories: analytical methods and iterative reconstruction algorithms [30]. This study focused on accurately obtaining the transmission measurement trajectory length and did not delve deeply into the intricacies of the reconstruction algorithm. The optimization of the algorithm will be discussed in future research. Consequently, for image reconstruction, the maximum likelihood expectation maximization (MLEM) algorithm was employed [31], and its iterative formula is expressed as follows [32, 33]:

$$\mu_j^{(k+1)} = \frac{\mu_j^{(k)}}{\sum_i T_{ij}} \sum_i T_{ij} \frac{p_i}{\sum_j T_{ij} \mu_j^{(k)}} \tag{14}$$

where  $k$  is the number of iterations of the algorithm,  $\mu_j^{(k)}$  is the estimated value of the line attenuation coefficients on all voxels during the  $k$ -th iteration,  $p_i$  is the projection value obtained during the  $i$ -th transmission measurement of the substance to be measured, and  $T_{ij}$  is the trajectory length value on the  $j$ -th voxel during the  $i$ -th measurement.

### 2.4 Image quality evaluation methods

To assess the quality of the reconstructed images of nuclear waste barrels, various evaluation methods are essential, including visual inspection and profiles for qualitative

assessment, and the mean square error (MSE) and signal-to-noise ratio (SNR) for quantitative analysis [34].

MSE indicates the difference between the reconstructed and reference images, and a smaller MSE value indicates a better quality of the reconstructed image. In this study, SNR was also employed to evaluate the noise level of the reconstructed image; higher SNR values corresponded to lower image noise.

The MSE and SNR are expressed in Eqs. (15), and (16):

$$MSE = \frac{1}{MN} \sum_{m=1}^M \sum_{n=1}^N (\mu_{Rec}(m, n) - \mu_{Ref}(m, n))^2 \tag{15}$$

$$SNR = 10 \log_{10} \left[ \frac{\sum_{m=1}^M \sum_{n=1}^N (\mu_{Ref}(m, n))^2}{\sum_{m=1}^M \sum_{n=1}^N (\mu_{Rec}(m, n) - \mu_{Ref}(m, n))^2} \right] \tag{16}$$

where  $\mu_{Rec}(m, n)$  is the reconstruction value of the  $m$ th row and  $n$ th column of the reconstructed image and  $\mu_{Ref}(m, n)$  is the reference value of the  $m$ th row and  $n$ th column of the reference image.

## 3 Result analysis and discussion

### 3.1 Simulation model of nuclear waste barrel

To evaluate the virtual trajectory length model, Geant4 was used to simulate the TGS system. Two models were designed in this study. The first model, labeled Model 1, was a nuclear waste barrel without concrete filling. It comprised four distinct materials: fiber, concrete, water, and aluminum. The geometric representation of Model 1 is shown in Fig. 2a. In addition, a second model, labeled Model 2, was developed to assess the practical applicability of the virtual trajectory length model. Model 2 was a nuclear waste barrel filled with concrete, as shown in Fig. 2b. The fibers were positioned at three specific locations within Model 2, and the remaining space outside these regions was filled with concrete. Reference images of nuclear waste barrels are required to evaluate the quality of the reconstructed transmission images [35]. In this study, parallel beam  $\gamma$ rays were used to irradiate the nuclear waste barrel model vertically. The intensities of the rays passing through the model at different positions were obtained, which facilitated the acquisition of a reference image of the nuclear waste barrel [36]. In the reference image, different colors represent distinct densities of the medium [37], as shown in Fig. 2c, d. Notably, in the projection calculations, the number of particles without attenuation is based on the number of particles passing through the barrel wall. The count after particle attenuation utilizes the particle count values of the particles passing through either

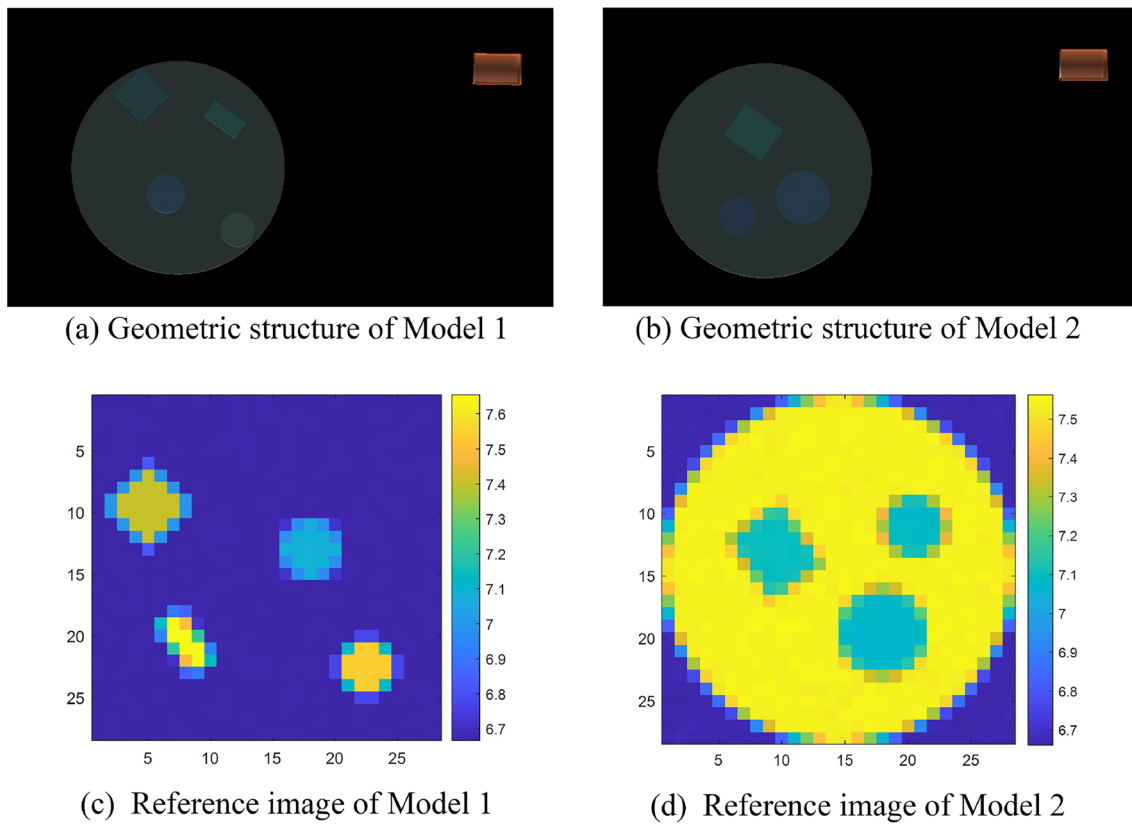


**Fig. 2** (Color online) Geometric structure of Model 1 and Model 2, and their reference images

Model 1 or Model 2. Consequently, the reconstructed image did not include the barrel wall, thus circumventing the potential influence of nuclear waste barrel walls on the results.

### 3.2 Comparison of different models for trajectory lengths

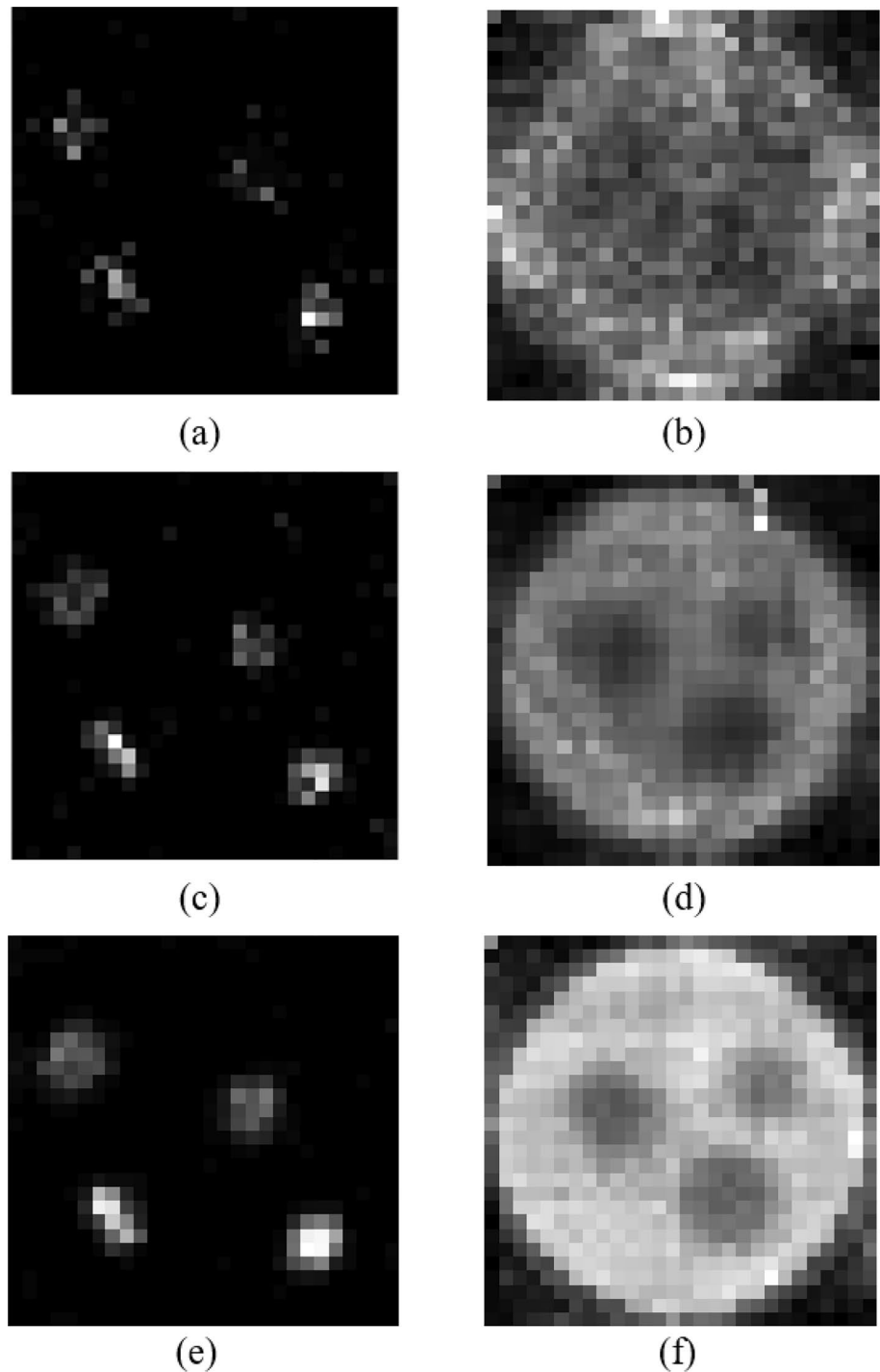
Two models were incorporated to validate the accuracy of the proposed trajectory length method. The first model was the “point-to-point” model established by Estep, and the second model was the average trajectory model proposed by Quanhu. These models provide additional trajectory length data for reference when a virtual model is used to extract trajectory lengths for image reconstruction. When reconstructing the images using trajectory lengths obtained from the “point-to-point” and average trajectory models, the projection data were not corrected for detection efficiency. However, when the virtual model was utilized for the trajectory length, the projection data were corrected for detection efficiency. The reconstruction images of Model 1 are labeled as Fig. 3a, c, e, and those of Model 2 are labeled as Fig. 3b, d, f.

### 3.3 Qualitative evaluation

In the reconstructed images (Fig. 3a) corresponding to the “point-to-point” model, the result appears unclear. They could not accurately capture the specific structure of the medium in Model 1. Conversely, the reconstruction image for the average trajectory length model shown in Fig. 3c provides a distinct representation of the structure of the medium. Therefore, the average trajectory length model exhibited superiority over the “point-to-point” model. In the reconstruction images (Fig. 3e), corresponding to the virtual trajectory length model, a visual inspection confirmed that the reconstructed medium (both shape and position) within the barrel was closer to the reference image of Model 1. This indicated a substantial improvement in the reconstructed images.

In the reconstruction images of Model 2 (Fig. 3b, d, f), it was evident apparent that, compared to the “point-to-point” and average trajectory length models, the virtual trajectory length model exhibited superior reconstruction quality. This model successfully reconstructed the filling material within the barrel and effectively restored pertinent information of the measured medium.

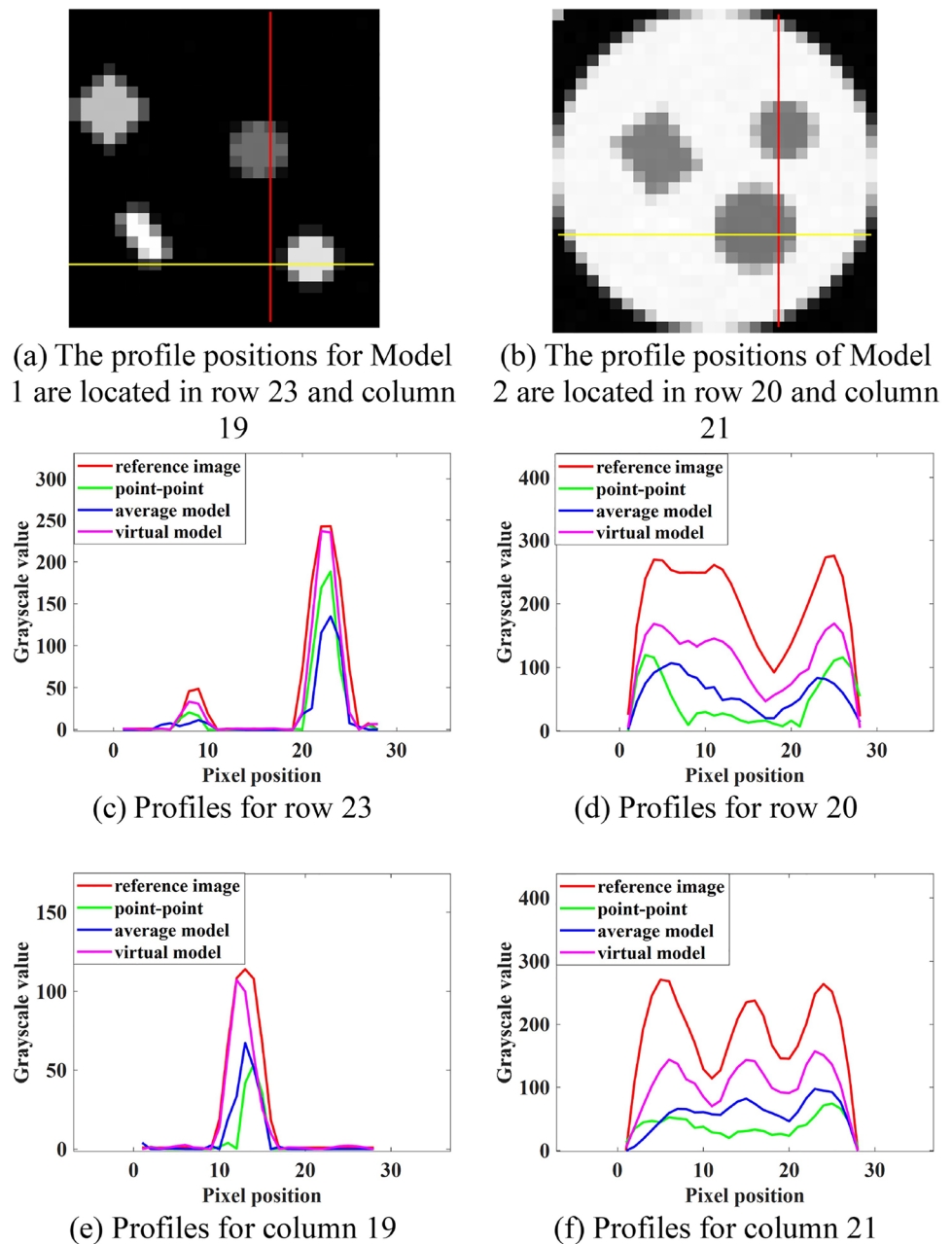
**Fig. 3** Reconstruction results of Models 1 and 2 under different trajectory length models. The results of Model 1 are shown in 1st column. The results of Model 2 are shown in 2nd column



The reconstruction and reference images' profiles of the two models are shown in Fig. 4c, e, and d, f, respectively. The positions of the profiles are presented in Fig. 4a, b. A comparison of the images revealed that the reconstructed images' profiles using the virtual trajectory length model exhibited a higher degree of consistency with the profile diagram of the reference image. The overall trends of their

profiles were closer and smoother, implying that the proposed virtual trajectory length model significantly reduced the noise level of the reconstructed images. The reconstruction results of the virtual trajectory length model exhibited a qualitative improvement, whether for assumed Model 1 or Model 2, which was closer to the real waste barrel environment.

**Fig. 4** (Color online) Comparison of reconstruction image' profiles



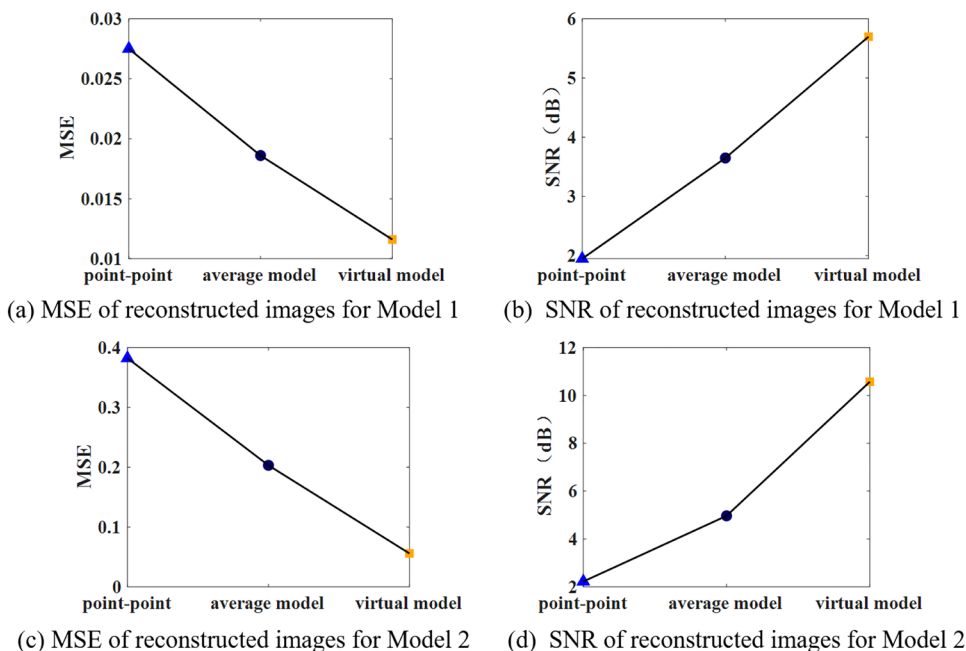
### 3.4 Quantitative evaluation

For the various trajectory length models, the MSE and SNR of the reconstructed images for both Models 1 and 2 are shown in Fig. 5:

In Fig. 5a, b, the virtual trajectory length model demonstrated significant advantages over the “point-to-point” and average trajectory length models for Model 1. Compared to the “point-to-point” model, the virtual trajectory length model reduced the MSE by 57.8% and increased the SNR by 192.3%. Further, the average trajectory length model, which addressed the overlooked solid angle problem inherent in the “point-to-point” model, yielded trajectory lengths that

were closer to the actual values. However, compared with the average model, the virtual trajectory length model proposed in this study still achieved a 37.6% reduction in MSE and a 56.1% improvement in SNR. This discrepancy can be attributed to the following factors. (1) The number of detector end-face grids. The process of numerous particles reaching the detector end face and being detected was simulated using a virtual trajectory length model. Notably, the number of end-face grids was considerably greater than that of the average model, reaching millions or even billions of levels (as determined by the number of emitted particles, more particles will lead to more grids). (2) Nonuniform detection efficiency. The proposed model considered the nonuniform

**Fig. 5** (Color online) MSE and SNR of reconstructed images under different trajectory length models



detection efficiency of the actual TGS detector end face. This resulted in a smaller deviation between the obtained and actual trajectory lengths.

In the objective assessment of the reconstruction results for Model 2, the virtual trajectory length model consistently demonstrated a superior reconstruction quality. Compared to the “point-to-point” and average trajectory models, the MSE decreased by 85.4% and 72.5%, respectively. In addition, the SNR increased by 375.0% and 112.7%, respectively. These results confirmed that the trajectory length model proposed in this study improved the quality of the reconstructed images and effectively reduced noise.

Based on the comprehensive qualitative and quantitative analyses conducted above, it can be concluded that the proposed virtual trajectory length model, which considers the nonuniform detection efficiency of the detector end face and the angular distribution of  $\gamma$ -rays at the detector, could accurately reconstruct the distribution of the medium within the nuclear waste barrel. The reconstruction quality achieved by this model was significantly superior to that of both the “point-to-point” and average trajectory models.

## 4 Conclusion

This study optimized the transmission reconstruction equation based on the actual situation of TGS transmission measurements. Consequently, a novel virtual trajectory length model was proposed. In contrast to conventional methods, such as the Cyrus–Beck algorithm, for calculating the equivalent trajectory length, this model leveraged the inherent characteristics of Geant4. A model was devised wherein a

multitude of particles traversed a virtual waste barrel and were subsequently detected, thereby yielding an equivalent track length. In contrast to the average model, this virtual trajectory length model featured more grids on the detector end face, effectively mitigating the effect of  $\gamma$ -rays on the angle distribution of the detector. Moreover, by considering the energy deposition process of each particle in the detector, it successfully circumvented the issue of nonuniform detection efficiency, as encountered in actual TGS detector end faces. The comparison results confirmed the capacity of the virtual trajectory length model to accurately reconstruct the medium distribution within the nuclear waste barrel, surpassing the performance of both the “point-to-point” and average trajectory models. Furthermore, the virtual trajectory length model proposed in this study will be extended to solve the emission track length, and an emission track length model including detection efficiency will be constructed to avoid complicated detector efficiency calibration during emission measurement.

**Author Contributions** All authors contributed to the study conception and design. Material preparation, data collection and analysis were performed by Rong-Rong Su, San-Gang Li and Chu-Xiang Zhao. The first draft of the manuscript was written by Rong-Rong Su, and all authors commented on previous versions of the manuscript. All authors read and approved the final manuscript.

**Data availability** The data that support the findings of this study are openly available in Science Data Bank at <https://cstr.cn/31253.11.sciencedb.15622> and <https://www.doi.org/10.57760/sciencedb.15622>.

## Declarations

**Conflict of interest** The authors declare that they have no conflict of interest.

## References

- J.Z. Zhang, X.G. Tuo, Geometric matrix research for nuclear waste drum tomographic gamma scanning transmission image reconstruction. *Chin. Phys. C* **39**, 068202 (2015). <https://doi.org/10.1088/1674-1137/39/6/068202>
- Lévai Ferenc, Low resolution combined emission-transmission imaging techniques for matrix characterization and assay of waste, in 17th Esarda Symposium, Aachen (1995)
- C.J. Chang, S. Anghaie, A high-definition gamma scanning method for the near-field nondestructive assay of large nuclear waste barrels. *Nucl. Technol.* **124**, 265–275 (2017). <https://doi.org/10.13182/NT98-A2925>
- J.C. Palacios, L.C. Longoria, J. Santos et al., A PC-based discrete tomography imaging software system for assaying radioactive waste containers. *Nucl. Instrum. Methods A* **508**, 500–511 (2003). [https://doi.org/10.1016/S0168-9002\(03\)00987-2](https://doi.org/10.1016/S0168-9002(03)00987-2)
- R. Venkataraman, M. Villani, S. Croft et al., An integrated tomographic gamma scanning system for non-destructive assay of radioactive waste. *Nucl. Instrum. Methods A* **579**, 375–379 (2007). <https://doi.org/10.1016/j.nima.2007.04.125>
- S.P. Narayanam, M. Manohari, R. Ramar et al., Monte Carlo simulation of an HPGe detector for detection of  $^{239}\text{Pu}$  in waste assay system. *Appl. Radiat. Isot.* **152**, 127–134 (2019). <https://doi.org/10.1016/j.apradiso.2019.07.003>
- R.L. Harrison, Simulation of medical imaging systems: emission and transmission tomography, in *Handbook of Particle Detection and Imaging*, 1–32 (2021). [https://doi.org/10.1007/978-3-319-47999-6\\_44-2](https://doi.org/10.1007/978-3-319-47999-6_44-2)
- Y.C. Yan, M.Z. Liu, X.Y. Li et al., Improved Cohen-Sutherland algorithm for TGS transmission imaging. *Nucl. Sci. Tech.* **34**, 98 (2023). <https://doi.org/10.1007/s41365-023-01238-8>
- M.M. Han, Z.R. Guo, H.F. Liu et al., Evaluation of an emission path length computation model applied at different resolutions in Tomographic Gamma Scanning. *Nucl. Instrum. Methods A* **927**, 267–279 (2019). <https://doi.org/10.1016/j.nima.2019.01.048>
- M.W. Rawool-Sullivan, R.J. Estep, Estimation of obliquely scattered gamma-ray response functions in the gross-count tomographic gamma scanner (GC-TGS) method. *IEEE Nucl. Sci. Symp. Conf. Rec.* **1**, 774–778 (1997). <https://doi.org/10.1109/NSSMIC.1997.672697>
- Z. Liu, L. Zhang, J. Hao, Radiation intensity image reconstruction in TGS using ART algorithm with geometrically-corrected system matrix and TV constraint, in *IEEE Nucl. Sci. Symp. Med. Imaging Conf. Rec.* 78–82 (2012). <https://doi.org/10.1109/NSSMIC.2012.6551064>
- D.C. Camp, H.E. Martz, G.P. Roberson et al., Nondestructive waste-drum assay for transuranic content by gamma-ray active and passive computed tomography. *Nucl. Instrum. Methods A* **495**, 69–83 (2002). [https://doi.org/10.1016/S0168-9002\(02\)01315-3](https://doi.org/10.1016/S0168-9002(02)01315-3)
- S. Croft, R. Venkataraman, M. Villani, On the accuracy of the tomographic gamma scanner for the assay of drummed waste. *Environm. Sci., Physics*, WM-4285 (2004)
- Satoru Kawasaki, Shigeru Izumi et al., Radioactivity measurement of drum package waste by a computed-tomography technique. *Int. J. Radiat. Appl. Instrum. A. Appl. Radiat. Isot.* **41**, 983–987 (1990). [https://doi.org/10.1016/0883-2889\(90\)90164-C](https://doi.org/10.1016/0883-2889(90)90164-C)
- R. Venkataraman, S. Croft, M. Villani et al., The next generation Tomographic Gamma Scanner. *Environm. Sci. Phys.* (2005)
- R.J. Estep, T.H. Prettyman, G.A. Sheppard, Tomographic Gamma Scanning to assay heterogeneous radioactive waste. *Nucl. Sci. Eng.* **118**, 145–152 (1994). <https://doi.org/10.13182/NSE94-A19380>
- W.Q. Weng, Reconstruction algorithm of transmission image in tomographic gamma scanning. Shanghai Jiao Tong University (2008) (in Chinese)
- J.A. Fessler, I.A. Elbakri, P. Sukovic et al., Maximum-likelihood dual-energy tomographic image reconstruction, in *SPIE Medical Imaging Proc. SPIE*, vol. 4684, (2002). <https://doi.org/10.1117/12.467189>
- M.M. Han, Novel edge treatment method for improving the transmission reconstruction quality in Tomographic Gamma Scanning. *Appl. Radiat. Isot.* **135**, 232–238 (2018). <https://doi.org/10.1016/j.apradiso.2018.02.006>
- T.H. Prettyman, R.A. Cole et al., A maximum-likelihood reconstruction algorithm for tomographic gamma-ray nondestructive assay. *Nucl. Instrum. Methods A* **356**, 470–475 (1995). [https://doi.org/10.1016/0168-9002\(94\)01352-7](https://doi.org/10.1016/0168-9002(94)01352-7)
- Z. Zhou, S.G. Li, Q.S. Tan et al., Optimization method of Hadamard coding plate in  $\gamma$ -ray computational ghost imaging. *J. Nucl. Sci. Tech.* **34**, 13 (2023). <https://doi.org/10.1007/s41365-022-01164-1>
- Q.H. Zhang, Research on Tomographic Gamma Scanning (TGS) reconstruction techniques. Doctoral dissertation. (2003) (in Chinese)
- J.Z. Zhang, Research on key technologies of gamma scanning for nuclear waste barrel chromatography. Chengdu University of Technology (2014) (in Chinese)
- R.J. Estep, TGS[FIT]: Image reconstruction software for quantitative, low-resolution tomographic assays. United States: N. (1993) <https://doi.org/10.2172/6779008>
- J.P. Wellisch, New trends in detector and background simulation: Geant4. *Czech J. Phys.* **56**, A173–A184 (2006). <https://doi.org/10.1007/s10582-006-0153-z>
- X.T. Ji, S.Y. Luo, Y.H. Huang et al., A novel 4D resolution imaging method for low and medium atomic number objects at the centimeter scale by coincidence detection technique of cosmic-ray muon and its secondary particles. *Nucl. Sci. Tech.* **33**, 2 (2022). <https://doi.org/10.1007/s41365-022-00989-0>
- E. Venialgo, M. Belzunce, C. Verrastrò et al., Analysis and comparison of Tomographic Gamma Scanner (TGS) architectures for nuclear waste characterization systems. *MMRS Online Proc. Libr.* **1475**, 533–538 (2012). <https://doi.org/10.1557/opl.2012.628>
- R.J. Estep, A preliminary design study for improving performance in tomographic assays. United States: N. (1994). <https://doi.org/10.2172/142477>
- S.I. Eidelman, B.A. Shwartz, Interactions of particles and radiation with matter, in *Handbook of Particle Detection and Imaging*, 3–24 (2021). <https://doi.org/10.1007/978-3-319-93785-4>
- L.Y. Huang, S.P. Zhu, T. Kuang, Simulation experiment of medical tomography image reconstruction. Xidian University Press (2015) (in Chinese)
- H.L. Zheng, Research on TGS image reconstruction technology for nuclear waste bins based on Proc Spie theory. China Academy of Engineering Physics (2019) (in Chinese)
- A.J. He, X.G. Tuo, R. Shi et al., MLEM image reconstruction algorithm for transmission Tomographic Gamma Scanning in drummed nuclear wastes. *Int. J. Appl. Sci. Eng. Technol.* **7**, 44–48 (2018). <https://doi.org/10.18483/ijSci.1640>
- J. Nuyts, D. Bequé, Image formation. *Med. Radiol. Diagn. Imaging* **17**, 291–310 (2006). [https://doi.org/10.1007/3-540-30005-8\\_17](https://doi.org/10.1007/3-540-30005-8_17)
- R. Shi, H.L. Zheng, X.G. Tuo et al., Image reconstruction based on total variation minimization for radioactive wastes Tomographic Gamma Scanning from sparse. *IEEE* **9**, 9 (2021). <https://doi.org/10.1109/ACCESS.2021.3088746>
- R.J. Estep, T.H. Prettyman, G.A. Sheppard, Comparison of attenuation correction methods for TGS and SGS: Do we really need

- selenium-75? Office of Scientific and Technical Information Technical Reports (1996)
36. Y. Liu, T.F. Zhu, Z. Luo et al., First-order primal-dual algorithm for sparse-view neutron computed tomography-based three-dimensional image reconstruction. *Nucl. Sci. Tech.* **34**, 118 (2023). <https://doi.org/10.1007/s41365-023-01258-4>
  37. Cédric. Carasco, Coupling gamma ray spectrometry and tomography in a Bayesian frame. *Nucl. Instrum. Methods A* **990**, 164985 (2021). <https://doi.org/10.1016/j.nima.2020.164985>
- Springer Nature or its licensor (e.g. a society or other partner) holds exclusive rights to this article under a publishing agreement with the author(s) or other rightsholder(s); author self-archiving of the accepted manuscript version of this article is solely governed by the terms of such publishing agreement and applicable law.